

Quantum tomography with τ leptons at the FCC-ee

Entanglement, Bell inequality violation, $\sin\theta_W$ and anomalous couplings

M. Fabbrichesi^a , and L. Marzola^{b,c} 

^a*INFN, Sezione di Trieste, Via Valerio 2, I-34127 Trieste, Italy*

^b*Laboratory of High-Energy and Computational Physics, NICPB, R vala 10, 10143 Tallinn, Estonia*

^c*Institute of Computer Science, University of Tartu, Narva mnt 18, 51009 Tartu, Estonia*

ABSTRACT

The Future Circular Collider (FCC)—in its first incarnation as a lepton collider—will produce, according to the proposed design, more than 100 billion pairs of τ leptons after working for four years at the energy of the Z -boson resonance. The τ lepton is special because its relatively long lifetime makes it possible to reconstruct the momenta of neutrinos emitted in the single pion decay mode. The resulting large number of events is an ideal source for a full quantum tomography of the process that will test quantum entanglement and the violation of Bell inequality with unprecedented precision. In addition, the study of polarizations and spin correlations can provide a competitive determination of the Weinberg angle θ_W and constrain possible anomalous couplings in the neutral electroweak current. We utilize analytic results and Monte Carlo simulations to explore to what extent these goals might be accomplished.



Contents

1	Motivations	3
2	Methods	3
2.1	Quantum tomography at work	4
2.2	Entanglement and Bell inequality violation	4
2.3	Monte Carlo simulation	7
2.3.1	Neutrino momenta reconstruction	8
2.3.2	Detector response and initial state radiation	8
3	Results	9
3.1	Theoretical quantum tomography: analytic results	10
3.2	Tomography with Monte Carlo simulation	12
3.2.1	Monte Carlo simulation with detector and ISR effects	12
3.2.2	Background and systematic uncertainties	13
3.3	Polarizations	13
3.3.1	The interplay between polarizations and entanglement	13
3.3.2	Weinberg angle	14
3.4	Anomalous couplings	14
3.4.1	Observables	15
3.4.2	Limits	15
4	Outlook	17

1 Motivations

THE STUDY OF THE τ LEPTON is interesting for at least three reasons. For a start, it is the heaviest among the leptons and for this reason alone a particle that deserves a detailed study. Next, an exact reconstruction of the neutrino momentum—and thereby that of the τ itself—is made possible by the relatively long lifetime that yields a measurable impact parameter for the charged pions produced in the semi-leptonic decay. Moreover, it decays into hadrons whose angular distribution of momenta allows for the reconstruction of the τ leptons polarization. The last two of these features make the quantum tomography of the corresponding polarization density matrix not only possible but also very precise.

The FCC-ee [1] is expected to produce 3×10^{12} visible Z after working for 4 years at the Z -boson resonance—of these 1.3×10^{11} will decay into τ -lepton pairs. Given the branching ratio of 10.82% for the single pronged charged pion plus a neutrino decay mode of the τ , we expect 1.7×10^9 events originated by the produced τ pairs. These events are the simplest to analyze, have very little if any background and also provide optimal resolution to analyze the polarization of the decaying leptons. For comparison, and to have a sense of the possible accomplishment, SuperKEKB [2] will produce by the end of its present run 5×10^{10} τ lepton pairs [3], while LEP produced about 137 000 of them [4]. For these reasons, the FCC-ee is the ideal laboratory for a detailed study of the τ lepton and of its properties fully accessible via quantum tomography.

The production of the τ pairs at the Z -boson resonance unveils the physics of the electroweak interactions and, in particular, the parity violating interactions yielding non-vanishing polarizations in the final state. These polarizations vanish in the lower energy regime where the photon dominates the production process. The interplay between polarizations and the other entries in the density matrix shows the origin, and the limited validity, of the maximum entanglement principle featured in purely electromagnetic processes—when only leptons are present. It also makes it possible to determine the Weinberg angle with great precision.

Finally, the definition of appropriated operators in terms of the polarization density matrix, leads to strong constraints on the size of the form factors of all operators up to dimension five affecting the electroweak neutral current. In the low-energy limit, these form factors correspond to the effective radius and magnetic and electric dipole momenta of the τ lepton.

Together with the above, perhaps more mundane goals, the FCC could push the study of quantum mechanics to regimes where it has yet to be fully investigated, namely at very high energies and in the presence of strong and electroweak interactions, opening the possibility of unexpected new fundamental discoveries.

2 Methods

THE DENSITY MATRIX OF A QUANTUM STATE can be fully reconstructed via a procedure dubbed quantum tomography. The τ leptons—whose spin states are represented by *qubits*, that is, two-level quantum states—act as their own polarimeters and the full polarization density matrix of a τ -lepton pair can be reconstructed by studying the angular distribution of suitable decay products. The simplest and most powerful—in terms of polarization resolution—of these decay modes is the single-prong $\tau \rightarrow \pi\nu_\tau$ decay. Other decay channels, including those yielding three pions or ρ or a_1 mesons, can also be used for quantum tomography purposes.

2.1 Quantum tomography at work

The density matrix describing the polarization state of a quantum system composed by two fermions can be written as

$$\rho = \frac{1}{4} \left[\mathbb{1} \otimes \mathbb{1} + \sum_i B_i^+ (\sigma_i \otimes \mathbb{1}) + \sum_j B_j^- (\mathbb{1} \otimes \sigma_j) + \sum_{i,j} C_{ij} (\sigma_i \otimes \sigma_j) \right], \quad (2.1)$$

with $i, j = r, n, k$ and σ_i being the Pauli matrices. The decomposition refers to a right-handed orthonormal basis, $\{\mathbf{n}, \mathbf{r}, \mathbf{k}\}$ and the quantization axis for the polarization is taken along \mathbf{k} , so that $\sigma_k \equiv \sigma_3$. In the fermion-pair center of mass frame we have

$$\mathbf{n} = \frac{1}{\sin \Theta} (\mathbf{p} \times \mathbf{k}), \quad \mathbf{r} = \frac{1}{\sin \Theta} (\mathbf{p} - \mathbf{k} \cos \Theta), \quad (2.2)$$

where \mathbf{k} is the direction of the τ^+ momentum and Θ is the scattering angle. We take $\mathbf{p} \cdot \mathbf{k} = \cos \Theta$, with \mathbf{p} being the direction of the incoming e^+ .

The coefficients B_i^\pm in Eq. (2.1) give the polarizations of the individual fermions, whereas the coefficients C_{ij} encode the spin correlations. By using $\text{Tr}(\sigma_i \sigma_j) = 2\delta_{ij}$ and $\text{Tr}(\sigma_i) = 0$, we have:

$$B_i^+ = \text{Tr}[\rho(\sigma_i \otimes \mathbb{1})], \quad B_i^- = \text{Tr}[\rho(\mathbb{1} \otimes \sigma_i)], \quad C_{ij} = \text{Tr}[\rho(\sigma_i \otimes \sigma_j)]. \quad (2.3)$$

More details on these definitions and quantum tomography in general can be found in [5].

The quantum tomography of the polarization density matrix is completed once the coefficients B_i and C_{ij} have been found. Given a Lagrangian for a theory, these quantities can be computed from the scattering amplitudes describing the underlying process. Experimentally, or in Monte Carlo simulations, they can instead be reconstructed by tracking the angular distribution of suitable τ -pair decay products. In particular, for events where each τ lepton decays to a single pion and a neutrino, we have

$$\frac{1}{\sigma} \frac{d\sigma}{d \cos \theta_i^\pm} = \frac{1}{2} (1 + B_i^\pm \cos \theta_i^\pm), \quad (2.4)$$

$$\frac{1}{\sigma} \frac{d\sigma}{d \cos \theta_i^+ d \cos \theta_j^-} = \frac{1}{4} (1 + C_{ij} \cos \theta_i^+ \cos \theta_j^-), \quad (2.5)$$

in which $\cos \theta_i^\pm$ are the projections of the π^\pm momentum direction on the $\{\mathbf{n}, \mathbf{r}, \mathbf{k}\}$ basis, as computed in the rest frame of the decaying τ^\pm . Figures 2.1 and 2.2 show the normalized distributions obtained for the values of the B_i and C_{ij} from the actual Monte Carlo simulation we have used in this work. The central values of the Gaussian fits—dashed lines—indicate the values of the coefficients themselves.

Whenever the average of the product of two cosine (in the C_{ij} coefficients) differ from the product of the averages of the single cosines (in the B_i coefficients) we have non vanishing correlation and, possibly, quantum entanglement.

2.2 Entanglement and Bell inequality violation

Given a two-qubit, 4×4 density matrix ρ as in (2.1), its *concurrence* can be explicitly constructed by using the auxiliary matrix

$$R = \rho (\sigma_y \otimes \sigma_y) \rho^* (\sigma_y \otimes \sigma_y), \quad (2.6)$$

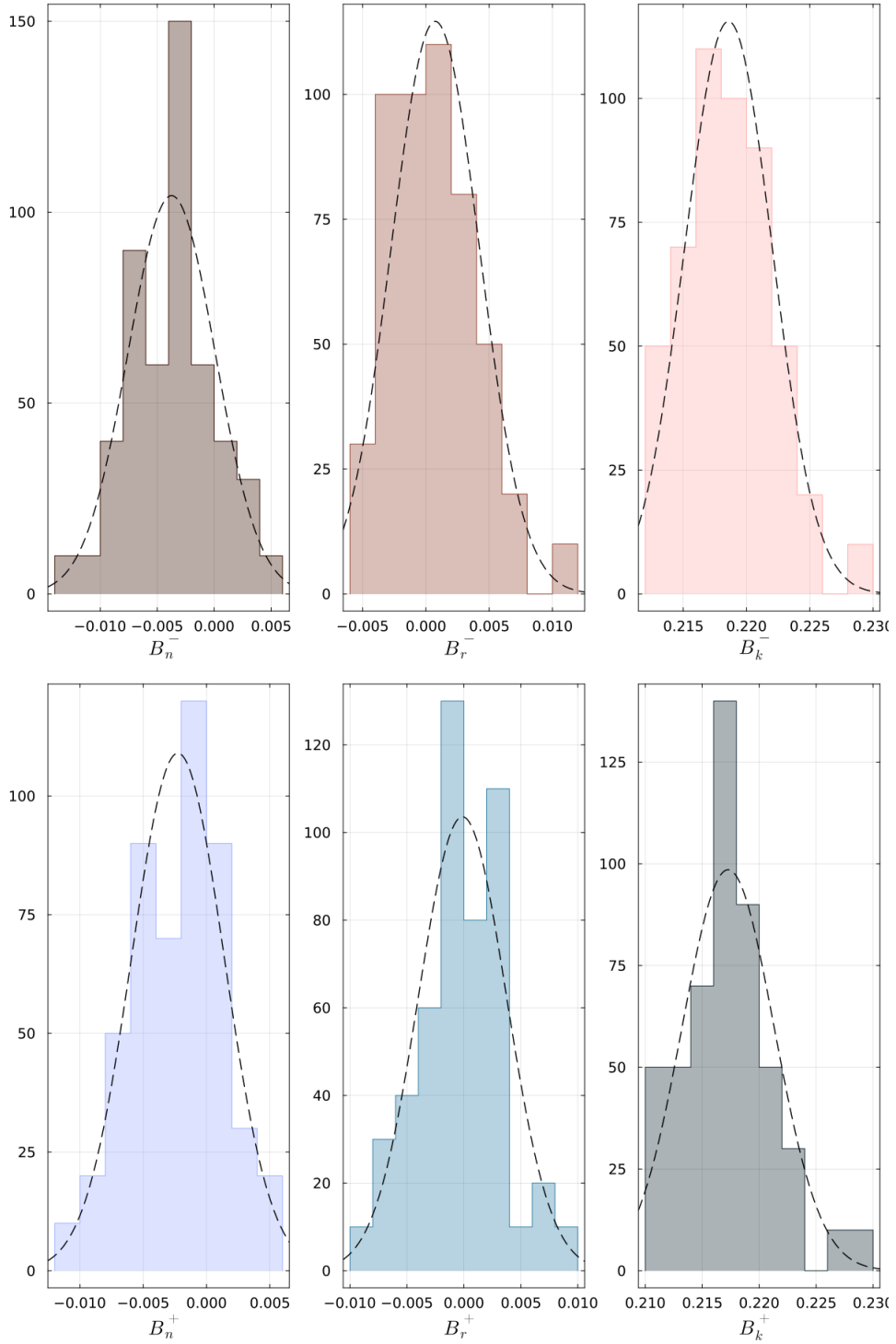


Figure 2.1: Distributions obtained for the coefficients B_i^\pm in the Monte Carlo simulation of the τ -lepton pairs decaying into a charged pion plus a neutrino, the momentum of which is reconstructed. The dotted curves represent the Gaussian fit of the histograms.

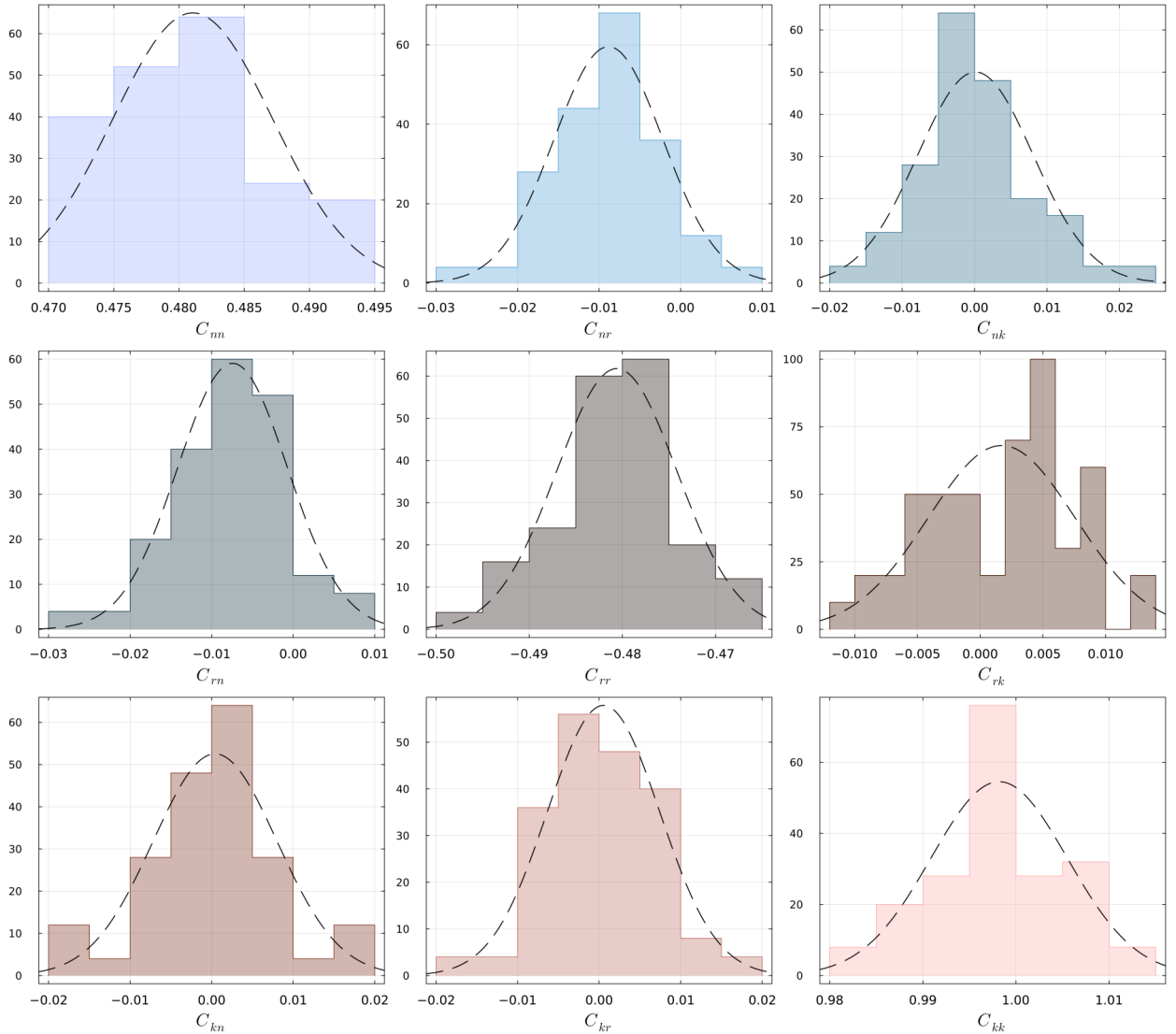


Figure 2.2: Distribution of the values of the coefficients C_{ij} in the Monte Carlo simulation of the τ -lepton pairs decaying into a charged pion plus a neutrino, the momentum of which is reconstructed. The dotted curves represent the Gaussian fit of the histograms.

where ρ^* denotes the matrix with complex conjugated entries. Although non-Hermitian, the matrix R has non-negative eigenvalues; denoting with r_i , $i = 1, 2, 3, 4$, their square roots and assuming r_1 to be the largest, the concurrence \mathcal{C} can be expressed as [6]

$$\mathcal{C} = \max(0, r_1 - r_2 - r_3 - r_4) . \quad (2.7)$$

The concurrence is a quantitative estimate of the amount of entanglement in the two-qubit system. Entanglement is present if $\mathcal{C} > 0$ and maximal for $\mathcal{C} = 1$.

To assess the possible violation of Bell inequalities we resort instead to the matrix C in Eq. (2.5) and build, with its transpose C^T , the symmetric, positive, 3×3 matrix $M = CC^T$; its eigenvalues m_1, m_2, m_3 can be ordered in increasing order: $m_1 \geq m_2 \geq m_3$. Then, the two-spin state ρ in (2.1) violates the Bell inequality [7], in its original as well as in the equivalent Clauser-Horne-Shimony-Holt

(CHSH) [8] form (for details see [5]) if and only if the sum of the two greatest eigenvalues of M is strictly larger than 1, that is (*Horodecki's condition* [9])

$$\mathbf{m}_{12} \equiv m_1 + m_2 > 1. \quad (2.8)$$

We take this condition as our test of the violation of the Bell inequality. It has the advantage of automatically maximize the amount of violation without having to worry about a specific choice of basis for the polarization vectors.

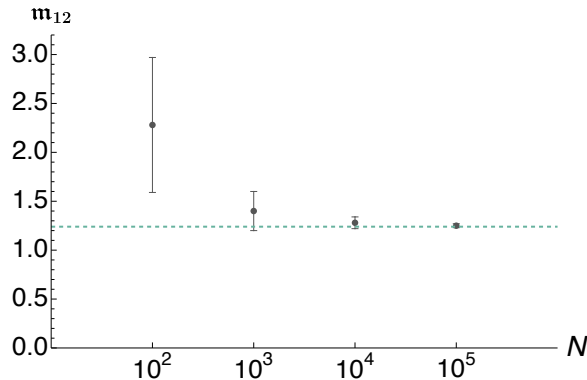


Figure 2.3: Numerical value of \mathbf{m}_{12} and its uncertainty obtained for the spin correlations of the τ -lepton pairs as the size N of the sample is varied. The dashed horizontal line corresponds to the analytic value. The bias is manifest for samples containing 100 events because \mathbf{m}_{12} must always be less than 2.

The Horodecki's condition in Eq. (2.8) may show a bias toward positive values when evaluated numerically on samples with a restricted statistics. The issue was addressed in [10] by correcting for it in the analysis of the violation of Bell inequalities in top-quark production at the LHC, a case in which the number of events is limited and \mathbf{m}_{12} is biased. In this work, as in [11], such a correction is not necessary because, as shown in Fig 2.3, the bias is negligible for samples containing at least 10^4 events.

2.3 Monte Carlo simulation

The Monte Carlo simulation provides all the inputs required for the quantum tomography of the process, which we perform as follows.

We generate 10 million events, containing each a τ lepton pair decaying into two opposite charged pions plus the τ neutrinos, by means of MADGRAPH5 [12] and the TAUDECAY library [13]. The events are generated at the tree level in the electroweak interaction and, therefore, the cross section and the remaining observables are expected to assume their tree-level values.

To make the simulation closer to the analysis with actual data, we replace the Monte Carlo truth τ lepton momenta with those obtained from the neutrino momenta reconstruction. We then sort the events into 50 independent samples (each corresponding to a pseudo-experiments with 2×10^5 events) and reconstruct the B_i^\pm and C_{ij} coefficients for each sample. The resulting Gaussian distributions, shown in Figures 2.1 and 2.2, give the central values and the statistical uncertainties of these parameters.

To mimic real data even further, we repeat the analysis by modelling the efficiency and uncertainty in the charged pion tracks and vertex determination of the detector prior to performing the neutrino momenta reconstruction. More details are given below.

2.3.1 Neutrino momenta reconstruction

The eight unknown components of the neutrino momenta can be reconstructed by means of eight equations: four from the sum of the τ -lepton momenta, which is constrained to satisfy

$$p_{\tau^+}^\mu + p_{\tau^-}^\mu = p_{e^+e^-}^\mu, \quad (2.9)$$

and four from the mass-shell conditions

$$(p_{\tau^+} - p_{\pi^+})^2 = m_\nu^2 = 0 \quad \text{and} \quad (p_{\tau^-} - p_{\pi^-})^2 = m_\nu^2 = 0 \quad (2.10)$$

$$p_{\tau^+}^2 = m_\tau^2 \quad \text{and} \quad p_{\tau^-}^2 = m_\tau^2. \quad (2.11)$$

The system of equations is second order and a two-fold degeneracy arises (see the Appendix in [14]).

As opposed to other processes, like top quark and W -boson decays, the reconstruction of the neutrino momenta and, therefore, of the τ momenta is almost perfect. The reason is that the τ lepton lives long enough to give a decay vertex that can be distinguished from the collision point. Consequently, the vector of closest approach, identified from the continuation of the trajectories of the pions emitted in the decay, can be measured and used as to resolve the two-fold degeneracy arising from the momenta reconstruction. Following [15], we then define the directions of the two charged pions as

$$\mathbf{n}_- = \frac{\mathbf{p}_-}{|\mathbf{p}_-|} \quad \text{and} \quad \mathbf{n}_+ = \frac{\mathbf{p}_+}{|\mathbf{p}_+|}, \quad (2.12)$$

in which \mathbf{p}_\pm are their momenta. The distance between the two decay vertices \mathbf{v}_\pm of the τ^\pm leptons is

$$\mathbf{d} = \mathbf{v}_+ - \mathbf{v}_-. \quad (2.13)$$

The vector of closest approach connecting the backward continuations of the two charged pion tracks is then given by

$$\mathbf{d}_{min} = \mathbf{d} + \frac{[(\mathbf{d} \cdot \mathbf{n}_+)(\mathbf{n}_- \cdot \mathbf{n}_+) - \mathbf{d} \cdot \mathbf{n}_-] \mathbf{n}_- + [(\mathbf{d} \cdot \mathbf{n}_-)(\mathbf{n}_- \cdot \mathbf{n}_+) - \mathbf{d} \cdot \mathbf{n}_+] \mathbf{n}_+}{1 - (\mathbf{n}_- \cdot \mathbf{n}_+)^2}. \quad (2.14)$$

The correct kinematic reconstruction of the τ momenta is then selected by computing \mathbf{d}_{min} for the two solutions and comparing the results with the measured value.

2.3.2 Detector response and initial state radiation

The performance of what will be the actual detectors of FCC-ee can only be presumed from the specifications detailed in the current experimental proposal.

The pairs of τ leptons must be identified from the charged pions appearing in the final state. Even though the efficiency is high but not 100%, this is not really a problem given the very large number of events available.

We model the detector resolution with the following uncertainties:

$$\frac{\sigma_{p_T}}{p_T} = 3 \times 10^{-5} \oplus 0.6 \times 10^{-3} \frac{p_T}{\text{GeV}} \quad \text{and} \quad \sigma_{\theta, \phi} = 0.1 \times 10^{-3} \text{ rad} \quad (2.15)$$

for the tracks proper and

$$\sigma_b = 3 \mu\text{m} \oplus \frac{15 \mu\text{m}}{\sin^{2/3} \Theta} \frac{\text{GeV}}{p_T} \quad (2.16)$$

for the impact parameters and for the reconstruction of the vector of closest approach. These values are taken from the envisaged IDEA tracking detector [1]; a constant smearing originates in imperfections in the detector or anomalies in signal collection, whereas the term scaling with the momentum is a noise that comes from the imperfection of the readouts. In the simulation we retain the leading contributions in the quoted uncertainties and account for the related detector effects by performing a Gaussian smearing of the Monte Carlo truth pion momenta and closest approach vector taking the nominal resolutions above as standard deviations.

Notice that the uncertainties are small if typical pion momenta of the order of 10 GeV and τ -lepton times of flight of the order of 0.1 mm are considered. Furthermore, the decay of the τ pairs will generally occur inside the beam pipe (of order 1 cm), thereby ensuring the absence of further interactions with the detector material that could quench the spin correlation under study.

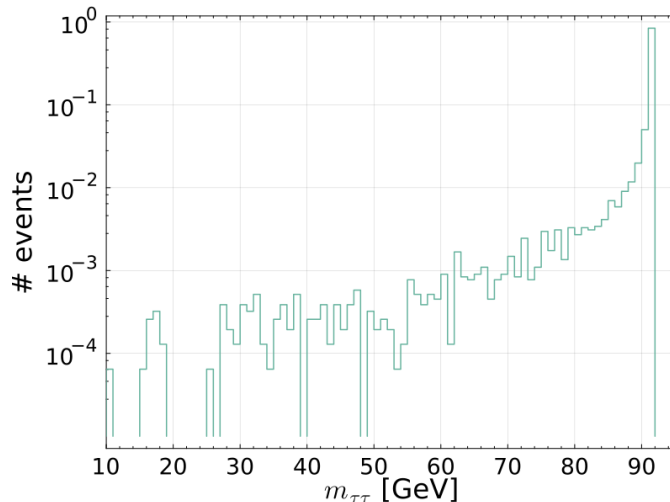


Figure 2.4: Distribution of the τ -lepton pair events in invariant mass after including the initial state radiation of the electrons. The last four bins, from 89 to 91 GeV, contain 99% of the events.

We also include in our Monte Carlo simulation the effect of Initial state radiation (ISR), which shifts the beam—and the actual center of mass (CM)—energy as shown in Fig. 2.4. The plot is obtained by using PYTHIA 8 [16] and following the indicated statistics we pollute our dataset with events characterized by a lower CM energy up to $\sqrt{s} = 89$ GeV, corresponding to the last three bins of Fig. 2.4 which comprise 99% of the events.

The angular distributions of the pion momenta in the rest frame of the τ -lepton pairs give, as the desired, the coefficients of the polarization density matrix. In the following we compare the results obtained from analytical computations to the values indicated by the Monte Carlo simulations performed with and without the ISR and detector resolution effects.

3 Results

QUANTUM TOMOGRAPHY gives us the means to study entanglement and Bell inequality violation in the process

$$e^+e^- \rightarrow Z \rightarrow \tau^+\tau^- \rightarrow \pi^+\pi^-\nu_\tau\bar{\nu}_\tau \quad (3.1)$$

as it will be available at the FCC-ee.

3.1 Theoretical quantum tomography: analytic results

Let us first look at the analytic results for the parton level process $e^+e^- \rightarrow Z \rightarrow \tau^+\tau^-$. This study already provides most of the information about the actual physical process, that is, the one inclusive of the hadronic decays of the τ leptons.

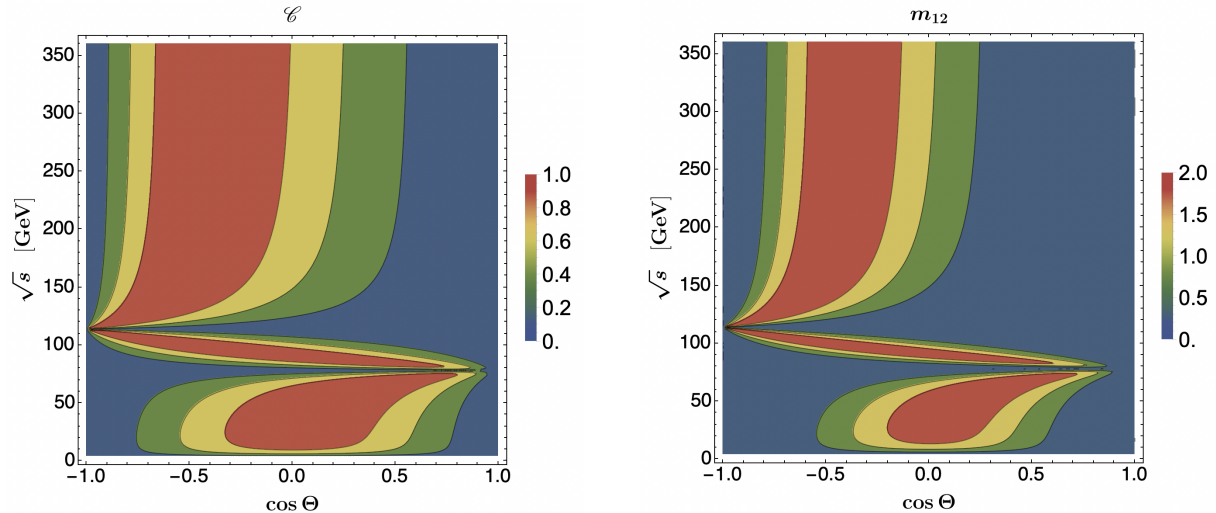


Figure 3.1: Analytic solutions for the concurrence (left) and the Bell inequality violation (right) in the parton level process $e^+e^- \rightarrow \tau^+\tau^-$. The presence of entanglement is signaled by $\mathcal{C} > 0$ and the violation of Bell inequalities by $m_{12} > 1$.

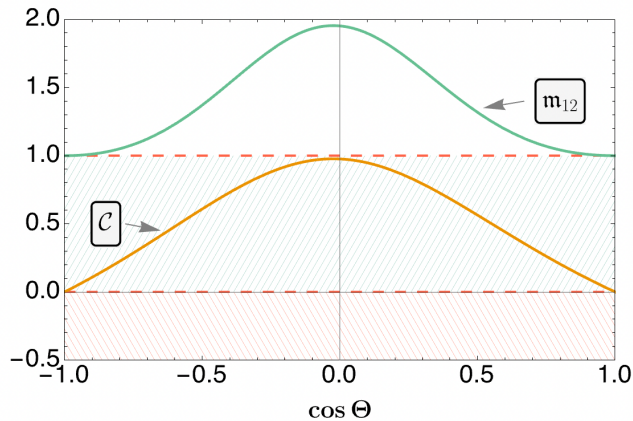


Figure 3.2: Values of the concurrence \mathcal{C} and the Horodecki's condition m_{12} as functions of the scattering angle in the parton level process $e^+e^- \rightarrow \tau^+\tau^-$. The presence of entanglement is signaled by $\mathcal{C} > 0$ and the violation of Bell inequalities by $m_{12} > 1$.

The values of the concurrence \mathcal{C} and the Horodecki's condition m_{12} for energies that range from the production threshold up to 350 GeV are shown in Fig. 3.1. The result for $\sqrt{s} = 10$ GeV have been already discussed in [11] and applied to superKEKB and the physics at Belle II. Here we study the region at the Z -boson resonance. In Fig. 3.2 the C M energy is set at $\sqrt{s} = 91.19$ GeV and the

concurrence and the Horodecki's condition are shown as functions of the scattering angle Θ , formed by the e^+ and τ^+ directions.

As for the polarization of the τ pair, we find $B_i^+ = B_i^- = B_i$ for $i = r, n, k$. Contrary to most of the other process that have been utilized in studies of entanglement, we have non vanishing B_i coefficients at the leading order even though the initial beam is made of unpolarized electrons and positrons. This feature is due to the parity violating electroweak interactions and makes the study of the τ leptons at this energy particularly interesting. The two plots in Fig. 3.3 show the behavior of the coefficients B_i^\pm as functions of the scattering angle Θ at $\sqrt{s} = 91.19$ GeV, as well as in a broader energy range.

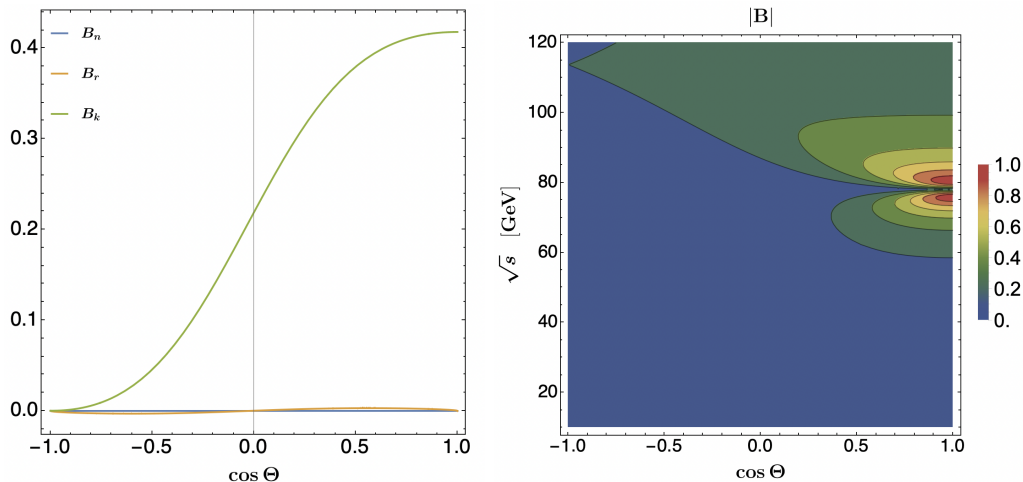


Figure 3.3: Coefficients $B_i = B_i^+ = B_i^-$ as functions of the scattering angle in the parton level process $e^+e^- \rightarrow \tau^+\tau^-$ at $\sqrt{s} = 91.19$ GeV (left) and $|B| = \sqrt{B_k^2 + B_n^2 + B_r^2}$ across a broader kinematic space (right).

The coefficients C_{ij} and B_i averaged over the angular distribution of the τ pair are found to be

$$C = \begin{pmatrix} 0.4878 & 0 & 0 \\ 0 & -0.4878 & 0.0011 \\ 0 & 0.0011 & 1 \end{pmatrix} \quad B^+ = B^- = \begin{pmatrix} 0 \\ 0.0001 \\ 0.2194 \end{pmatrix}. \quad (3.2)$$

These values can be directly compared with the results of the Monte Carlo simulations. We find that the system is entangled and that the weighted angular averaged value of the concurrence is

$$\mathcal{C} = 0.4878. \quad (3.3)$$

As shown in Fig 3.2 the entanglement depends on the kinematic region and is maximal at $\Theta = \pi/2$.

Similarly, the violation of the Bell inequality is given by

$$\mathbf{m}_{12} = 1.238, \quad (3.4)$$

which again, is the result for the angular average, and can be enhanced by choosing a kinematic region around $\Theta = \pi/2$ (see Fig. 3.2).

While the analytic results show evidence for entanglement and Bell inequality violation, a quantitative study requires an estimate of the related uncertainties inherent to the experimental analyses. For these, we turn to the Monte Carlo simulation.

3.2 Tomography with Monte Carlo simulation

As explained in Section 2, we generate a total of 10^7 events containing τ pairs that result in two opposite charged pions and missing energy in the final states. For each of the events we reconstruct the rest frames of the τ^\pm leptons and compute the projection of their spin, indicated by the directions of the pions, on the $\{\mathbf{r}, \mathbf{n}, \mathbf{k}\}$ basis in these frames of reference. The statistical uncertainty is estimated by running 50 independent pseudo-experiments each consisting of a sample of 200 000 events drawn from the full dataset of 10^7 Monte Carlo generated events.

Omitting, for the moment, the effects of ISR and finite detector resolution, the procedure leads to the following determination of the coefficients C_{ij} and their statistical uncertainty:

$$C = \begin{pmatrix} 0.4810 \pm 0.0061 & -0.0089 \pm 0.0067 & -0.0001 \pm 0.0080 \\ -0.0074 \pm 0.0068 & -0.4806 \pm 0.0065 & 0.0017 \pm 0.0059 \\ 0.0004 \pm 0.0076 & 0.0005 \pm 0.0069 & 0.9982 \pm 0.0073 \end{pmatrix}. \quad (3.5)$$

For the coefficients B_i we have:

$$B^+ = \begin{pmatrix} -0.0023 \pm 0.0037 \\ -0.0001 \pm 0.0039 \\ 0.2173 \pm 0.0040 \end{pmatrix} \quad B^- = \begin{pmatrix} -0.0037 \pm 0.0038 \\ 0.0007 \pm 0.0035 \\ 0.2186 \pm 0.0035 \end{pmatrix}. \quad (3.6)$$

The concurrence is found to be

$$\mathcal{C} = 0.481 \pm 0.004, \quad (3.7)$$

and the Horodecki's condition for the violation of the Bell inequality is given by

$$\mathbf{m}_{12} = 1.233 \pm 0.014. \quad (3.8)$$

The values in Eqs. (3.7)–(3.8) are in excellent agreement with the analytic results, proving that the size of the samples used in the analysis yields sufficient precision.

3.2.1 Monte Carlo simulation with detector and ISR effects

To have a better sense of the actual experimental uncertainties, we run a second Monte Carlo simulation including the smearing of the charged pion momenta and of the closest approach vector discussed in Section 2.3, and contaminating the sample with events at lower \sqrt{s} to include the effect of ISR. This procedure gives

$$C = \begin{pmatrix} 0.4819 \pm 0.0079 & -0.0073 \pm 0.0082 & -0.0016 \pm 0.0089 \\ -0.0066 \pm 0.0082 & -0.4784 \pm 0.0084 & 0.0016 \pm 0.0070 \\ -0.0002 \pm 0.0080 & -0.0004 \pm 0.0087 & 1.000 \pm 0.0074 \end{pmatrix} \quad (3.9)$$

$$B^+ = \begin{pmatrix} -0.0028 \pm 0.0042 \\ -0.0001 \pm 0.0049 \\ 0.2198 \pm 0.0044 \end{pmatrix} \quad B^- = \begin{pmatrix} -0.0039 \pm 0.0048 \\ 0.0017 \pm 0.0049 \\ 0.2207 \pm 0.0044 \end{pmatrix}. \quad (3.10)$$

According to the above results for the coefficients C_{ij} and B_i , we find that the concurrence is given now by

$$\mathcal{C} = 0.4805 \pm 0.0063 \quad (3.11)$$

and the Horodecki's condition by

$$\mathbf{m}_{12} = 1.239 \pm 0.017. \quad (3.12)$$

The significance of the Bell inequality violation is about 14 standard deviations. Equations Eqs. (3.11)–(3.12) are the main result of the present work. The significance can be increased by means of kinematic cuts that select events with scattering angles close to $\Theta = \pi/2$, for which the values of \mathcal{C} and \mathbf{m}_{12} are larger (see Fig. 3.2).

3.2.2 Background and systematic uncertainties

The dominant background arises from misconstruction of the τ decay channel. This is very small for the single pion channel, much smaller than for other decay channels as that into two pions. A potentially large background comes from the presence of electron and positrons in the final state, but it can be controlled by using the impact parameter. Backgrounds arising from the process $e^+e^- \rightarrow q\bar{q}$ and from other sources are even smaller. We therefore feel that it is not necessary to estimate their effect for the purpose of the present analysis.

The absolute value of the difference between the central values of the concurrence obtained in the Monte Carlo simulation without, see Eq. (3.7), and with detector effects and ISR, see Eq. (3.11), is

$$\delta\mathcal{C}|_{\text{syst}} = |0.481 - 0.485| = 0.004; \quad (3.13)$$

similarly, for the Horodecki condition signaling the violation of the Bell inequality (cf. Eqs. (3.8)–(3.12)) we have

$$\delta\mathbf{m}_{12}|_{\text{syst}} = |1.233 - 1.239| = 0.006. \quad (3.14)$$

These differences provide an estimate of the upper bound in the systematic errors of these two observables. They are subdominant with respect to the statistical errors in Eq. (3.11) and Eq. (3.12).

To find the expected uncertainty at the FCC-ee—where about 10^9 events are to be collected in four years of operation—we must rescale our uncertainties obtained by running pseudo-experiments containing 200 000 event each by a factor $10\sqrt{50}$. This rescaling will make the statistical uncertainties smaller than the upper limits on the systematic errors, which at that point will come to dominate the overall uncertainty unless reduced and brought under control. We expect that indeed this will be the case and that the systematic error will be under control after the operating of the machine and the detectors are comprehensively understood.

3.3 Polarizations

The coefficients B_i^\pm are directly related to the polarizations of the τ leptons. Analytically, we find that these coefficients are equal, $B_i^+ = B_i^-$ for $i = r, n, k$.

From the Monte Carlo simulation with detector effects and ISR included, we take the polarization to be the arithmetic average and obtain

$$\boxed{\langle P \rangle_\tau = \frac{1}{2}(B_k^+ + B_k^-) = 0.2203 \pm 0.0044,} \quad (3.15)$$

while B_n^\pm and B_r^\pm are consistent with their vanishing analytic value, and the overall sign depends on the frame of reference. The polarization in Eq. (3.15) corresponds to the tree-level value, the measured value being 0.1476 ± 0.0108 [4].

3.3.1 The interplay between polarizations and entanglement

The components B_i of the polarization and the coefficients C_{ij} of the spin correlations are closely related, for they both enter the density matrix which must satisfy positivity and normalization conditions. The entanglement is the largest for vanishing polarizations and vice versa. This relationship

explains the maximum entanglement shown by amplitudes in parity conserving theories, such as QED [17], that have vanishing polarizations. This also happens in electroweak processes if the parity violating structure of the lepton current is suppressed, as it is known to be for the special, and unphysical, choice $\sin \theta_W = 0.5$ [17]. For this value, the vector coupling of leptons vanishes and the current conserves parity. The cancellation is not possible for any common value of the Weinberg angle once quark currents are involved because of the different charges. For this reason, the requirement of maximum entanglement (or the vanishing of the polarizations, which amounts to the same), though appealing, can hardly be promoted to a general principle from which to constrain a Standard Model parameters like the Weinberg angle itself.

3.3.2 Weinberg angle

The Weinberg angle can be obtained from the polarization vector P_τ using the relation [18]

$$P_\tau(\cos \Theta) = \frac{\mathcal{A}_\tau (1 + \cos^2 \Theta) + 2 \cos \Theta \mathcal{A}_e}{1 + \cos^2 \Theta + 2 \cos \Theta \mathcal{A}_\tau \mathcal{A}_e}, \quad (3.16)$$

with,

$$\mathcal{A} = \mathcal{A}_e = \mathcal{A}_\tau = \frac{2(1 - 4 \sin^2 \theta_W)}{1 + (1 - 4 \sin^2 \theta_W)^2}, \quad (3.17)$$

assuming lepton flavor universality.

We compute the Weinberg angle by taking the weighted angular average of Eq. (3.16) and finding \mathcal{A} by solving the equation after inserting the value of $\langle P \rangle_\tau$ from Eq. (3.15). Inserting the value of \mathcal{A} so obtained into Eq. (3.17) yields the equation

$$0.2190 = \frac{2(1 - 4 \sin^2 \theta_W)}{1 + (1 - 4 \sin^2 \theta_W)^2}, \quad (3.18)$$

which shows that the uncertainty in the coefficient B_i is reduced by a factor of about 8 in the error propagation. The central value for the Weinberg angle that solves Eq. (3.18) corresponds to the tree level value:

$$\boxed{\sin^2 \theta_W = 0.2223 \pm 0.0006}, \quad (3.19)$$

consistently with the inputs of our Monte Carlo simulation.

Assuming that the systematic uncertainties will eventually be under control, we rescale the uncertainty of our sample to account for the expected FCC-ee yield and obtain an uncertainty of 7.8×10^{-6} on the determination of the tree-level Weinberg angle. This uncertainty is two order of magnitude better than the current value [19]. The report [1] cites uncertainties in the Weinberg angle determination between 10^{-5} and 10^{-6} as one of the goals for the FCC-ee machine.

3.4 Anomalous couplings

The τ lepton—the heaviest among the leptons, as the top quark among the quarks—could be the likeliest to show a behavior departing from that described by the Standard Model. The most general electroweak Lorentz-invariant vertex Γ^μ between the Z -boson and the τ lepton up to dimension five operators can be written as

$$i \frac{g}{2 \cos \theta_W} \bar{\tau} \Gamma^\mu(q^2) \tau Z_\mu(q) = i \frac{g}{2 \cos \theta_W} \bar{\tau} \left[\gamma^\mu F_1^V(q^2) + \gamma^\mu \gamma_5 F_1^A(q^2) + \frac{i \sigma^{\mu\nu} q_\nu}{2m_\tau} F_2(q^2) + \frac{\sigma^{\mu\nu} \gamma_5 q_\nu}{2m_\tau} F_3(q^2) \right] \tau Z_\mu(q), \quad (3.20)$$

with $F_1^V(0) = g_V = -1/2 + 2 \sin^2 \theta_W$ and $F_1^A(0) = -g_A = 1/2$. $F_2(0)$ is the magnetic and $F_3(0)$ the electric dipole moment. We parametrize the first two form factors in terms of a Taylor expansion as

$$F_1^{V,A}(q^2) = F_1^{V,A}(0) + \frac{q^2}{m_Z^2} C_1^{V,A}, \quad (3.21)$$

and give limits on the coefficients $C_1^{V,A}$ at $q^2 = m_Z^2$. These form factors act as anomalous couplings of the τ lepton to the Z boson.

3.4.1 Observables

Our strategy to constrain the form factors in Eq. (3.20) exploits the polarization density matrix, which can be experimentally reconstructed through quantum tomography and gives a bird's-eye view of the possible observables available for a given process.

The method has been previously used to constrain physics beyond the SM affecting the top-quark [20, 21] and τ pair [21] production at the LHC and at superKEKB [22], or yielding Higgs anomalous couplings to τ leptons [14] and gauge bosons [23–25].

For the present case, we use the entries of the polarization density matrix to define three observables that provide the means to best constrain the parameters in Eq. (3.20): one observable is the concurrence \mathcal{C} defined in Eq. (2.7) and it measures the entanglement in the spin states of the produced τ pairs, another—specific to the CP-violating contributes—is related to triple products involving one momentum and the spin vectors of the τ leptons:

$$\mathcal{C}_{odd} = \sum_{i < j} |C_{ij} - C_{ji}|, \quad (3.22)$$

and the third is the total cross section:

$$\sigma_T = \frac{1}{64\pi^2 s} \int d\Omega \frac{|\mathcal{M}|^2}{4} \sqrt{1 - \frac{4m_\tau^2}{s}}, \quad (3.23)$$

in which we neglect the electron mass and take $\sqrt{s} = 91.19$ GeV.

3.4.2 Limits

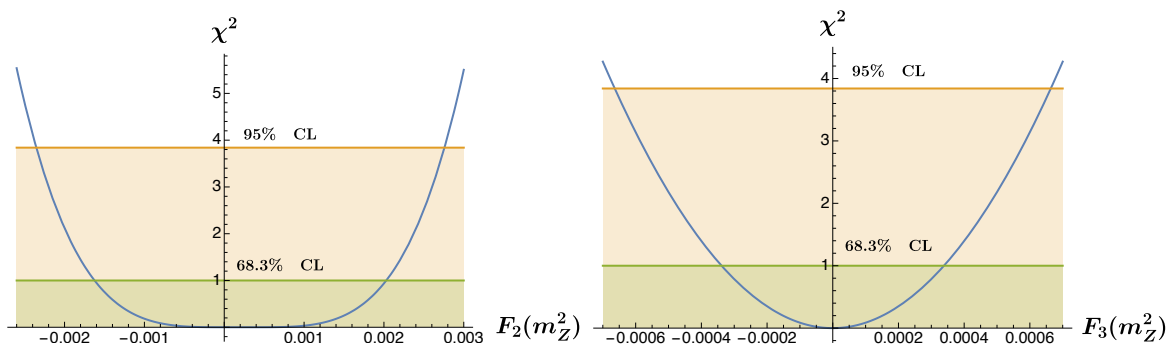


Figure 3.4: χ^2 test for the form factor $F_2(m_Z^2)$ and $F_3^V(m_Z^2)$. The limits for $F_2(m_Z^2)$ are obtained by means of the concurrence, those for the form factor $F_3^V(m_Z^2)$ by means of the operator \mathcal{C}_{odd} .

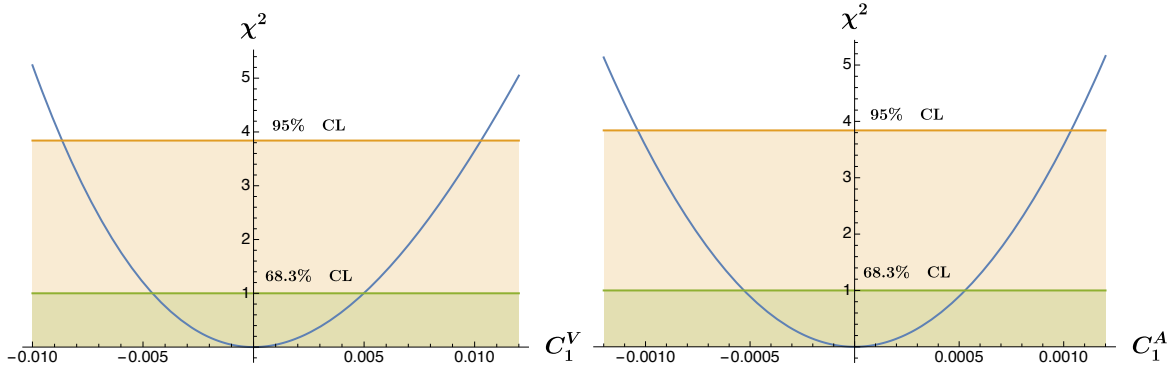


Figure 3.5: χ^2 test for the form factor $F_1^V(m_Z^2)$ (left) and $F_1^A(m_Z^2)$ (right). Both limits are obtained by means of the cross section.

\mathcal{O}_a	σ_a	form factor limits
\mathcal{C}	0.006	$-0.002 \leq F_2(m_Z^2) \leq 0.003$
\mathcal{C}_{odd}	0.009	$-0.001 \leq F_3(m_Z^2) \leq 0.001$
σ_T	0.05 pb	$-0.009 \leq C_1^V \leq 0.010$
σ_T	0.05 pb	$-0.001 \leq C_1^A \leq 0.001$

Table 3.1: Bounds obtained at the 95% confidence level for the form factors, as shown in Figures 3.4 and 3.5, neglecting correlations. The values refer to a sample of 200 000 events; limits for larger samples can be obtained by rescaling these values by the square root of the ratio of the corresponding numbers of events.

For a sample of 200.000 events, the expected value and uncertainty on the cross section is (22.83 ± 0.05) pb. For the same sample, from Section 3.2.1, we find an uncertainty on C_{ij} , and therefore on \mathcal{C}_{odd} , of at most 0.009, and on the concurrence \mathcal{C} of 0.006. We use these uncertainties in the determination of the limits on the form factors with the understanding that they can be improved by rescaling the number of events to that actually expected at the FCC-ee.

The operators introduced in the previous section, generically denoted here as $\mathcal{O}_a[F_i(m_Z^2)]$, depend on the electroweak form factors $F_i(m_Z^2)$ and \mathcal{O}_{SM} are the values of the operators for the Standard Model. To constrain the couplings, we introduce a χ^2 test set for a (68.3) 95% C.L.

$$\left[\frac{\mathcal{O}_a[F_i(m_Z^2)] - \mathcal{O}_{SM}}{\sigma_a} \right]^2 \leq (1.00) 3.84, \quad (3.24)$$

in which we set the uncertainties σ_a for the operators \mathcal{O}_a at the values discussed in the previous paragraph.

The bounds on each coupling can be extracted from Fig. 3.4 and 3.5 under the assumption that the parameters are independent. With that, we neglect possible correlations. The values obtained from the 95% confidence interval are reported in Table 3.1.

In Table 3.1 we report the limits as obtained with the most effective operator. For the form factor $F_2(m_Z^2)$, we could have included those obtained with the cross section instead of the concurrence. The cross section provides a slightly stronger bound because it has a smaller relative uncertainty. This does not mean that the cross section is a more sensitive observable than the concurrence. Fig. 3.6 shows that the limits from the concurrence are stronger than those from the cross section when a common relative uncertainty is considered.

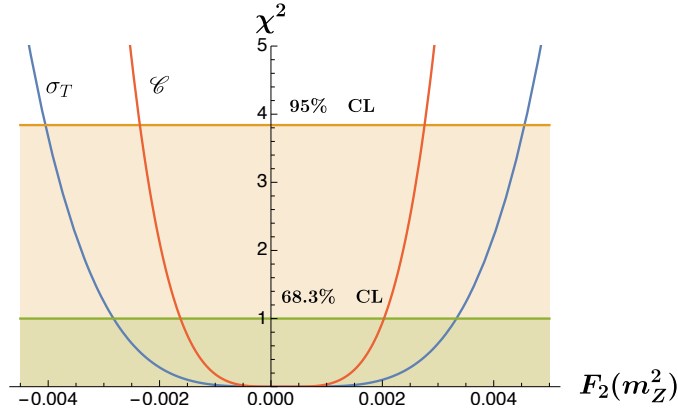


Figure 3.6: The χ^2 tests for the form factor $F_2^V(m_Z^2)$ using the cross section (σ_T) and the concurrence (\mathcal{C}) show that the latter provides more stringent limits when equal relative uncertainties are considered.

The limit on $F_3(m_Z^2)$ in Table 3.1 corresponds to a limit on the CP violating weak dipole moment of 5.6×10^{-18} e cm for the τ lepton. The corresponding limit from LEP is equal to 1.4×10^{-17} [26, 27]. These limits are comparable since they are obtained with a similar number of events and utilize similar observables built out of a CP-odd triple product. Rescaling our limits to the FCC-ee luminosity, we find $|F_3(m_Z^2)| \leq 2.0 \times 10^{-19}$, which is one order of magnitude better than the current limit: 3.6×10^{-18} e cm [19].

Table 3.1 shows the bounds obtained with pseudo-experiments containing each 200 000 events. Corresponding projections base on the full dataset of 10^9 expected at the FCC-ee can be derived (considering only the statistical errors) upon a rescaling by a factor $10\sqrt{50}$.

4 Outlook

THE FCC-EE CAN, after 4 years of operation at the energy of the Z -boson mass, test quantum entanglement and Bell inequality violation in τ -lepton pairs with extraordinary precision. Already with the reduced sample we have used in our analysis the significance is well in excess of five standard deviations and it is expected to reach many times that value with the full expected dataset of 10^9 events—provided the systematic uncertainties are under control. We believe that the results we have presented make a convincing case for including the quantum tomography of the τ leptons in the physics goals of the FCC-ee. The work also proves that the same quantum tomography technique can provide new and stringent bounds on the form factors entering the electroweak neutral current of the τ leptons.

Acknowledgements

The authors thank Michele Pinamonti and Christian Veelken for discussions. L.M. is supported by the Estonian Research Council grants PRG803, RVT3 and by the CoE program grant TK202 “Fundamental Universe”.

References

- [1] **FCC** Collaboration, A. Abada et al., *FCC-ee: The Lepton Collider: Future Circular Collider Conceptual Design Report Volume 2*, *Eur. Phys. J. ST* **228** (2019), no. 2 261–623.
- [2] SuperKEKB Collaboration, *SuperKEKB Collider*, *Nucl. Instrum. Meth. A* **907** (2018) 188, [arXiv:1809.01958].
- [3] **Belle-II** Collaboration, W. Altmannshofer et al., *The Belle II Physics Book*, *PTEP* **2019** (2019), no. 12 123C01, [arXiv:1808.10567]. [Erratum: *PTEP* 2020, 029201 (2020)].
- [4] **L3** Collaboration, M. Acciarri et al., *Measurement of tau polarization at LEP*, *Phys. Lett. B* **429** (1998) 387–398.
- [5] A. J. Barr, M. Fabbrichesi, R. Floreanini, E. Gabrielli, and L. Marzola, *Quantum entanglement and Bell inequality violation at colliders*, arXiv:2402.07972.
- [6] W. K. Wootters, *Entanglement of formation of an arbitrary state of two qubits*, *Phys. Rev. Lett.* **80** (Mar, 1998) 2245–2248.
- [7] J. Bell, *On the Einstein Podolsky Rosen paradox*, *Physics Physique Fizika* **1** (1964) 195.
- [8] J. F. Clauser, M. A. Horne, A. Shimony, and R. A. Holt, *Proposed experiment to test local hidden variable theories*, *Phys. Rev. Lett.* **23** (1969) 880–884.
- [9] R. Horodecki, P. Horodecki, and M. Horodecki, *Violating bell inequality by mixed spin-1/2 states: necessary and sufficient conditions*, *Phys. Lett. A* **200** (1995) 340.
- [10] M. Fabbrichesi, R. Floreanini, and G. Panizzo, *Testing Bell Inequalities at the LHC with Top-Quark Pairs*, *Phys. Rev. Lett.* **127** (2021), no. 16 161801, [arXiv:2102.11883].
- [11] K. Ehatäht, M. Fabbrichesi, L. Marzola, and C. Veelken, *Probing entanglement and testing Bell inequality violation with $e^+e^- \rightarrow \tau^+\tau^-$ at Belle II*, *Phys. Rev. D* **109** (2024), no. 3 032005, [arXiv:2311.17555].
- [12] J. Alwall, R. Frederix, S. Frixione, V. Hirschi, F. Maltoni, O. Mattelaer, H. S. Shao, T. Stelzer, P. Torrielli, and M. Zaro, *The automated computation of tree-level and next-to-leading order differential cross sections, and their matching to parton shower simulations*, *JHEP* **07** (2014) 079, [arXiv:1405.0301].
- [13] K. Hagiwara, T. Li, K. Mawatari, and J. Nakamura, *TauDecay: a library to simulate polarized tau decays via FeynRules and MadGraph5*, *Eur. Phys. J. C* **73** (2013) 2489, [arXiv:1212.6247].
- [14] M. M. Altakach, P. Lamba, F. Maltoni, K. Mawatari, and K. Sakurai, *Quantum information and CP measurement in $H \rightarrow \tau^-\tau^+$ at future lepton colliders*, *Phys. Rev. D* **107** (2023), no. 9 093002, [arXiv:2211.10513].
- [15] J. H. Kuhn, *Tau kinematics from impact parameters*, *Phys. Lett. B* **313** (1993) 458–460, [hep-ph/9307269].
- [16] C. Bierlich et al., *A comprehensive guide to the physics and usage of PYTHIA 8.3*, *SciPost Phys. Codeb.* **2022** (2022) 8, [arXiv:2203.11601].
- [17] A. Cervera-Lierta, J. I. Latorre, J. Rojo, and L. Rottoli, *Maximal Entanglement in High Energy Physics*, *SciPost Phys.* **3** (2017), no. 5 036, [arXiv:1703.02989].
- [18] S. Jadach and E. Was, *The τ polarization measurement*, in *Z PHYSICS AT LEP-1* (G. Altarelli, R. Kleiss, and C. Verzegnassi, eds.), p. 235. CERN-EP-89-129, 1989.
- [19] **Particle Data Group** Collaboration, R. L. Workman and Others, *Review of Particle Physics*, *PTEP* **2022** (2022) 083C01.
- [20] R. Aoude, E. Madge, F. Maltoni, and L. Mantani, *Quantum SMEFT tomography: Top quark pair production at the LHC*, *Phys. Rev. D* **106** (2022), no. 5 055007, [arXiv:2203.05619].
- [21] M. Fabbrichesi, R. Floreanini, and E. Gabrielli, *Constraining new physics in entangled two-qubit systems: top-quark, tau-lepton and photon pairs*, *Eur. Phys. J. C* **83** (2023), no. 2 162, [arXiv:2208.11723].
- [22] M. Fabbrichesi and L. Marzola, *Dipole momenta and compositeness of the τ lepton at Belle II*, arXiv:2401.04449.
- [23] M. Fabbrichesi, R. Floreanini, E. Gabrielli, and L. Marzola, *Stringent bounds on HWW and HZZ anomalous couplings with quantum tomography at the LHC*, *JHEP* **09** (2023) 195, [arXiv:2304.02403].
- [24] A. Bernal, P. Caban, and J. Rembieliński, *Entanglement and Bell inequalities violation in $H \rightarrow ZZ$ with anomalous coupling*, *Eur. Phys. J. C* **83** (2023), no. 11 1050, [arXiv:2307.13496].

- [25] R. Aoude, E. Madge, F. Maltoni, and L. Mantani, *Probing new physics through entanglement in diboson production*, *JHEP* **12** (2023) 017, [[arXiv:2307.09675](#)].
- [26] **OPAL** Collaboration, P. D. Acton et al., *Test of CP invariance in $e^+e^- \rightarrow \tau^+\tau^-$ and a limit on the weak dipole moment of the tau lepton*, *Phys. Lett. B* **281** (1992) 405–415.
- [27] **ALEPH** Collaboration, D. Buskulic et al., *Search for CP violation in $Z \rightarrow \tau\tau$* , *Phys. Lett. B* **297** (1992) 459–468.